

Theoretical Analysis of Transient Conjugate Convective Heat Transfer Induced by Interfacial Heat Sources in Channels

Jianqiang Liu^{1,2}, Xiaodong Ruan^{1,2}, Jing Wang^{1,2}, Rui Su^{1,2}, Yingnan Shen^{1,2}, Liang Hu^{1,2}

¹State Key Laboratory of Fluid Power and Mechatronics Systems, Zhejiang University
Hangzhou, China

²Engineering Research Center of DLIS, Ministry of Education
China

liujianqiang0329@zju.edu.cn; xdruan@zju.edu.cn; jing.wang@zju.edu.cn;
srhello@zju.edu.cn; shenyngnan@zju.edu.cn; cmeehuli@zju.edu.cn

Abstract - The problem of transient conjugate convective heat transfer in a parallel plate channel under laminar flow conditions, induced by a heat source at the fluid-solid interface is investigated in this study. Utilizing the thermal quadrupole theory and a two-dimensional numerical Laplace inverse transform method, the transient temperature fields in both the solid and fluid domains were successfully derived. To validate the accuracy of the semi-analytical solutions, a comparison was conducted with finite element numerical simulations, demonstrating strong agreement between the two approaches. Based on the semi-analytical solutions, the spatiotemporal evolution of the temperature fields in the fluid and solid domains induced by the interfacial heat source was preliminarily analysed. Furthermore, the spatiotemporal coupling of heat flux transfer between the fluid and solid domains was examined, resulting in the development of a directional map of spatiotemporal heat flux during the transient heat transfer process. This map reveals the complex relationship between the heat flux density at the fluid-solid interface and its spatiotemporal directionality, providing significant insights for transient heat transfer analysis in such problems.

Keywords: transient conjugate convective heat transfer; fluid-solid interface; semi-analytical solutions; heat source

1. Introduction

Conjugate heat transfer problems induced by interfacial heat sources at the fluid-solid interface represent a critical area of heat transfer research with widespread engineering applications. Researchers have investigated these problems using experimental, theoretical, and numerical approaches, which can be categorized into steady-state and transient studies. Among these, steady-state studies are relatively comprehensive, systematically addressing conjugate heat transfer problems induced by interfacial heat sources under three convective heat transfer modes: natural convection, forced convection, and mixed convection. The primary research motivation originates from the thermal management of packaged electronic components. For instance, T. A. Alves and C. A. C. Altemani conducted numerical simulations to study steady-state conjugate heat transfer induced by a 2D strip heat source in a finite-thickness parallel plate channel wall [1], conjugate heat transfer induced by a single interfacial heat source under laminar plug flow in parallel plate channels [2], and conjugate heat transfer with three discrete interfacial heat sources under plug flow or fully developed laminar forced convection in parallel plate channels [3]. Similarly, H. Bhowmik, C. P. Tso, K. W. Tou, and F. L. Tan experimentally investigated general convective heat transfer in a vertical rectangular channel with water as the working fluid for four simulated electronic chips, covering natural convection, mixed convection, and forced convection conditions [4].

Although steady-state studies are relatively extensive, as described in Ref. [5], time-varying systems are far more common in nature than time-invariant systems. However, due to computational challenges, difficulties, and costs, research on time-varying systems remains scarce. Nevertheless, certain engineering heat transfer analyses require a focus on transient heat transfer processes, such as heat transfer analysis in immersion flow field [6]. Particularly during exposure processes, on one hand, accumulated exposure heat at the fluid-silicon interface affects the temperature stability and uniformity of the liquid lens through convective heat transfer [7]; on the other hand, it influences the temperature uniformity of the silicon wafer through heat conduction, potentially causing thermal deformation of the wafer. Addressing this issue, A. Wei, A. Abdo, G. Nellis, R. Engelstad, J. Chang, E. Lovell, and W. Beckman [8] simulated the thermal effects of exposure energy on the immersion flow field during a single scanning cycle and the cumulative effects of exposure energy on silicon wafer heating during global scanning. Despite these efforts, transient conjugate heat transfer problems in parallel plate channels

induced by fluid-solid interfacial heat sources remain underexplored in theoretical analysis. The spatiotemporal coupling of heat flux transfer between fluid and solid during transient heat transfer processes also remains unclear.

As described in Ref. [9-10], compared to numerical simulation techniques such as finite element methods, the thermal quadrupole theory offers two significant advantages. First, through semi-analytical solutions, it enables rapid and efficient computation of the field of interest at specified locations and times. Second, it allows the solution of heat transfer problems involving arbitrarily stacked solid or fluid layers. Therefore, to address the aforementioned issues, this study applies the thermal quadrupole method proposed by G. Maranzana, I. Perry, and D. Maillet [11], combined with the 2D numerical Laplace inverse transform technique proposed by ISEGER [12], to theoretically solve the transient conjugate heat transfer problem in parallel plate channels induced by interfacial heat sources. Furthermore, the reliability of the semi-analytical solutions is validated through simulations. Finally, based on the theoretical solutions, the spatiotemporal coupling process of heat flux transfer between the fluid and solid is analysed, and a directional map of spatiotemporal heat flux during the transient heat transfer process induced by interfacial heat sources is provided.

2. Theoretical Analysis

2.1. Mathematic model

Fig. 1 illustrates the schematic diagram of conjugate convective heat transfer between fluid and solid in a channel induced by an interfacial heat source. The fluid enters the channel with uniformly distributed thermophysical and flow parameters at the inlet, and after passing through the entrance region, hydrodynamically fully developed laminar flow is established. The fluid is assumed to be an incompressible Newtonian fluid with constant thermophysical properties. Also, the flow is considered no-slip and viscous dissipation is neglected.

In addition, for ease of analysis in the following sections, the time domain is divided into three regions based on the start and end times of the interfacial heat source $I(t)$: Time I ($0 \leq t < t_0$): initial time domain; Time II ($t_0 \leq t < t_1$): heat application time domain; Time III ($t_1 \leq t < \infty$): heat decay time domain. Similarly, the spatial domain is divided into three regions based on the start and end locations of the interfacial heat source $I(t)$: Region I ($0 \leq x < x_0$): upstream region; Region II ($x_0 \leq x < x_1$): heat application region; Region III ($x_1 \leq x < \infty$): downstream region.

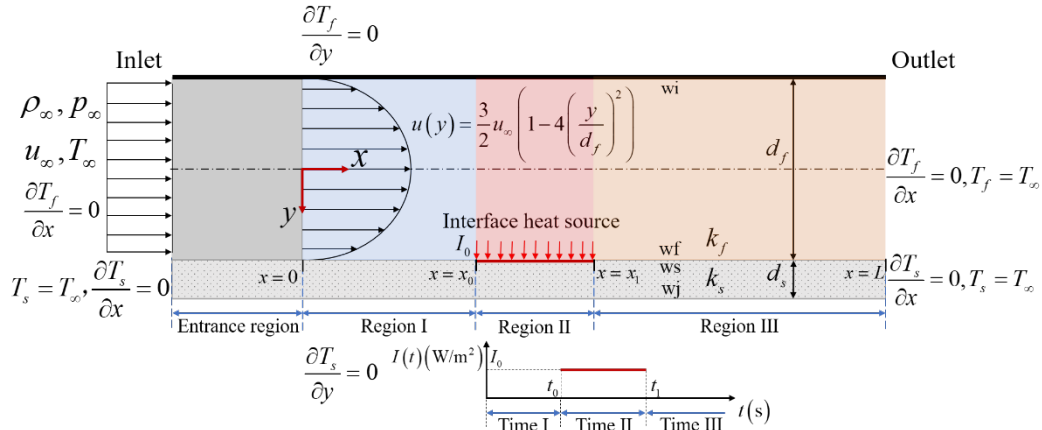


Fig. 1: Schematic of conjugate convective heat transfer problem induced by interfacial heat source.

Based on the aforementioned assumptions, the transient energy equation and velocity distribution in the fluid region can be expressed as follows respectively:

$$\frac{\partial T_f(x, y, t)}{\partial t} + u(y) \frac{\partial T_f(x, y, t)}{\partial x} = a_f \left(\frac{\partial^2 T_f(x, y, t)}{\partial x^2} + \frac{\partial^2 T_f(x, y, t)}{\partial y^2} \right) \quad (1)$$

$$u(y) = \frac{3}{2} U_\infty \left(1 - 4 \left(\frac{y}{d_f} \right)^2 \right) \quad (2)$$

Where $T_f(x, y, t)$, a_f are the transient temperature and the thermal expansion coefficient of fluid respectively, $u(y)$, U_∞ are the velocity in the axial direction and the bulk velocity respectively, d_f represents the channel height.

Similarly, the transient energy equation in the solid region can be expressed as:

$$\frac{\partial T_s(x, y, t)}{\partial t} = a_s \left(\frac{\partial^2 T_s(x, y, t)}{\partial x^2} + \frac{\partial^2 T_s(x, y, t)}{\partial y^2} \right) \quad (3)$$

Where $T_s(x, y, t)$, a_s are the transient temperature and the thermal expansion coefficient of solid respectively.

The boundary conditions and initial conditions for the above equations are as follows:

$$T_f(x, y, t)|_{x=0, L} = T_\infty; T_s(x, y, t)|_{x=0, L} = T_\infty \quad (4)$$

$$\frac{\partial T_f(x, y, t)}{\partial x} \Big|_{x=0, L} = 0; \frac{\partial T_s(x, y, t)}{\partial x} \Big|_{x=0, L} = 0 \quad (5)$$

$$\frac{\partial T_f(x, y, t)}{\partial x} \Big|_{y=-\frac{d_f}{2}} = 0; \frac{\partial T_s(x, y, t)}{\partial x} \Big|_{y=d_s+\frac{d_f}{2}} = 0 \quad (6)$$

$$T_f(x, y, t)|_{t=0} = T_\infty; T_s(x, y, t)|_{t=0} = T_\infty \quad (7)$$

Where the channel length L should go to infinity.

In addition, the continuity conditions at the fluid-solid interface are satisfied:

$$T_s(x, y, t)|_{y=\frac{d_f}{2}} = T_f(x, y, t)|_{y=\frac{d_f}{2}} \quad (8)$$

$$I(t) \cdot R(x) = -k_s \frac{\partial T_s(x, y, t)}{\partial y} \Big|_{y=\frac{d_f}{2}} + k_f \frac{\partial T_f(x, y, t)}{\partial y} \Big|_{y=\frac{d_f}{2}}; I(t) = \Re(t-t_0) - \Re(t-t_1), R(x) = \Re(x-x_0) - \Re(x-x_1) \quad (9)$$

Here k_f, k_s are the thermal conductivity of the fluid and solid respectively, \Re is the Heaviside function.

2.2. Analytical approximation

To facilitate the solution of the above energy equation, the following temperature rise variable $\theta(x, y, t)$ and its corresponding heat flux expression $\varphi(x, y, t)$ are defined:

$$\theta(x, y, t) = T(x, y, t) - T_\infty, \varphi(x, y, t) = -k \frac{\partial \theta(x, y, t)}{\partial y} \quad (10)$$

The following Laplace transform is introduced:

$$\bar{\theta}(s) = \int_0^\infty \theta(t) e^{-st} dt \quad (11)$$

$$\tilde{\theta}(p) = \int_0^\infty \theta(x) e^{-px} dx \quad (12)$$

Combining equation (10) and applying the aforementioned Laplace transform to the variables t and x in the energy equations (1) and (3), respectively, yields:

$$\frac{d^2 \tilde{\tilde{\theta}}_f}{dy^2} - \Upsilon^2 \tilde{\tilde{\theta}}_f = 0, \Upsilon^2 = \frac{s}{a_f} + \frac{u(y)p}{a_f} - p^2 \quad (13)$$

$$\frac{d^2 \tilde{\tilde{\theta}}_s}{dy^2} - \Omega^2 \tilde{\tilde{\theta}}_s = 0, \Omega^2 = \frac{s}{a_s} - p^2 \quad (14)$$

Before solving equation (13), the fluid domain is uniformly divided into K fluid sublayers, each with a thickness of Δd_K . The velocity of the k -th fluid sublayer can be expressed as:

$$u_k = \frac{3}{2} U_\infty \left(1 - \frac{4K}{3} \left(\frac{y_k^3 - y_{k-1}^3}{d_f^3} \right) \right) \quad (15)$$

Then, the energy equation for the k -th fluid sublayer can be expressed as:

$$\frac{d^2 \tilde{\theta}_{f_k}}{dy^2} - \Upsilon_k^2 \tilde{\theta}_{f_k} = 0, \Upsilon_k^2 = \frac{s}{a_f} + \frac{p}{a_f} u_k - p^2 \quad (16)$$

Finally, based on the thermal quadrupole method [11], the matrix relationship between the temperature rise $\tilde{\theta}$ and heat flux $\tilde{\varphi}$ on surfaces wi and wf in the Laplace domain can be obtained as:

$$\begin{bmatrix} \tilde{\theta} \\ \tilde{\varphi} \end{bmatrix}_{wi} = \begin{bmatrix} A_{f_1} & B_{f_1} \\ C_{f_1} & D_{f_1} \end{bmatrix} \cdots \begin{bmatrix} A_{f_k} & B_{f_k} \\ C_{f_k} & D_{f_k} \end{bmatrix} \cdots \begin{bmatrix} A_{f_k} & B_{f_k} \\ C_{f_k} & D_{f_k} \end{bmatrix} \begin{bmatrix} \tilde{\theta} \\ \tilde{\varphi} \end{bmatrix}_{wf} \quad (17)$$

Where $A_{f_k} = \cosh(\Upsilon_k \Delta d_k)$, $B_{f_k} = \frac{\sinh(\Upsilon_k \Delta d_k)}{k_f \Upsilon_k}$, $C_{f_k} = k_f \Upsilon_k \sinh(\Upsilon_k \Delta d_k)$, $D_{f_k} = \cosh(\Upsilon_k \Delta d_k)$.

Similarly, the matrix relationship between the temperature rise $\tilde{\theta}$ and heat flux $\tilde{\varphi}$ on surfaces ws and wj in the Laplace domain can be obtained as:

$$\begin{bmatrix} \tilde{\theta} \\ \tilde{\varphi} \end{bmatrix}_{ws} = \begin{bmatrix} A_s & B_s \\ C_s & D_s \end{bmatrix} \begin{bmatrix} \tilde{\theta} \\ \tilde{\varphi} \end{bmatrix}_{wj} \quad (18)$$

Where $A_s = \cosh(\Omega d_s)$, $B_s = \frac{\sinh(\Omega d_s)}{k_s \Omega}$, $C_s = k_s \Omega \sinh(\Omega d_s)$, $D_s = \cosh(\Omega d_s)$.

At the fluid-solid interface, the matrix relationship between surface wf and surface ws is expressed as:

$$\begin{bmatrix} \tilde{\theta} \\ \tilde{\varphi} \end{bmatrix}_{wf} = \begin{bmatrix} \tilde{\theta} \\ \tilde{\varphi} \end{bmatrix}_{ws} - \begin{bmatrix} 0 \\ \overline{IR} \end{bmatrix} \quad (19)$$

Furthermore, combining equations (17)–(19), the matrix relationship between surfaces wi and wj can be derived as:

$$\begin{bmatrix} \tilde{\theta} \\ \tilde{\varphi} \end{bmatrix}_{wi} = \begin{bmatrix} A_f & B_f \\ C_f & D_f \end{bmatrix} \left(\begin{bmatrix} A_s & B_s \\ C_s & D_s \end{bmatrix} \begin{bmatrix} \tilde{\theta} \\ \tilde{\varphi} \end{bmatrix}_{wj} - \begin{bmatrix} 0 \\ \overline{IR} \end{bmatrix} \right) \quad (20)$$

Where $\begin{bmatrix} A_f & B_f \\ C_f & D_f \end{bmatrix} = \begin{bmatrix} A_{f_1} & B_{f_1} \\ C_{f_1} & D_{f_1} \end{bmatrix} \cdots \begin{bmatrix} A_{f_k} & B_{f_k} \\ C_{f_k} & D_{f_k} \end{bmatrix} \cdots \begin{bmatrix} A_{f_k} & B_{f_k} \\ C_{f_k} & D_{f_k} \end{bmatrix}$.

Then, combining the boundary condition (5), i.e., $\tilde{\varphi}_{wi} = 0$ and $\tilde{\varphi}_{wj} = 0$, the temperature rise and heat flux expressions for the k -th fluid layer surface in the Laplace domain can be obtained as:

$$\tilde{\theta}_k = \frac{A_s D_k}{C_f A_s + D_f C_s} \overline{IR} \quad (21)$$

$$\tilde{\varphi}_k = -\frac{A_s C_k}{C_f A_s + D_f C_s} \overline{IR} \quad (22)$$

Similarly, the temperature rise and heat flux expressions for the solid domain in the Laplace domain can be obtained as:

$$\tilde{\theta}_s = \cosh(\Omega(d_s - y)) \frac{D_f}{C_f A_s + D_f C_s} \overline{IR} \quad (23)$$

$$\tilde{\varphi}_s = k_s \Omega \sinh(\Omega(d_s - y)) \frac{D_f}{C_f A_s + D_f C_s} \overline{IR} \quad (24)$$

Using the two-dimensional numerical Laplace inverse transform method proposed by ISEGER [12], the temperature rise and heat flux in the Laplace domain can be inversely transformed to obtain the temperature rise and heat flux in the fluid and solid domains.

3. Results and discussion

3.1. Numerical verification

To validate the accuracy of the semi-analytical solutions obtained using the thermal quadrupole method, finite element numerical simulations of the above conjugate heat transfer problem were conducted using the commercial software COMSOL Multiphysics. In the simulations, boundary layer meshing was applied to the upper and lower walls of the fluid domain, and a mesh independence test was performed. The final mesh consisted of 160,066 elements. In addition, the geometric parameters, flow parameters, and thermophysical properties used in both the finite element simulations and the thermal quadrupole method are summarized in Table 1.

Table 1: Parameters involved in theoretical solutions and finite element numerical simulations.

| Geometric parameters | values | Thermo-physical parameters | values | Numerical Laplace Inverse Transform parameters | values | Flow parameters and others | values |
|----------------------|----------|----------------------------|------------------------|--|---------|----------------------------|---------------------------|
| d_f | 0.0031 m | k_f | 0.6 W/(m·K) | M_1 | 512 | U_∞ | 0.23894 m/s |
| d_s | 0.0021 m | k_s | 1.4 W/(m·K) | M_2 | 512 | T_∞ | 295.15 K |
| x_0 | 0.026 m | ρ_s | 2200 kg/m ³ | n | 16 | I_0 | 30489.51 W/m ² |
| x_1 | 0.052 m | ρ_f | 1000 kg/m ³ | Δt | 0.1 s | t_0 | 1 s |
| L | 0.1 m | C_{pf} | 4180 J/(Kg·K) | Δx | 0.001 m | t_1 | 3 s |
| | | C_{ps} | 670 J/(Kg·K) | | | K | 20 |
| | | ν | 9.358E-4 Pa·s | | | | |

Fig. 2 illustrates the comparison of temperature responses obtained from COMSOL numerical simulations and thermal quadrupole theory at various spatial locations within the fluid and solid domains, along with their absolute error distributions. The results demonstrate a good agreement between the two methods. Additionally, from Fig. 2(b), 2(d), 2(f) and 2(h), it can be observed that the primary discrepancies occur near $t_1=3s$. This is attributed to the finite length ($L=0.1m$) used in the simulation model, which differs from the theoretical assumption of $L \rightarrow \infty$.

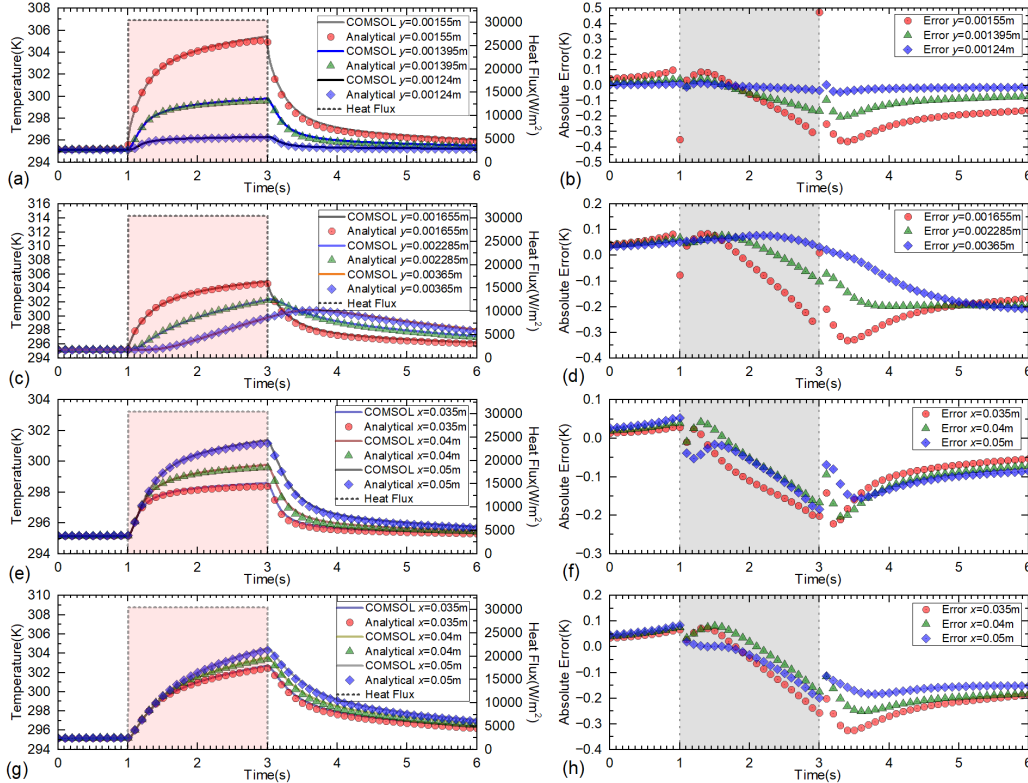


Fig. 2: Comparison of COMSOL and semi-analytical solutions for temperature at different locations, along with their absolute errors: (a) and (b) correspond to $x=0.04m$, at different vertical positions in the fluid domain; (c) and (d) correspond to $x=0.04m$, at different vertical positions in the solid domain; (e) and (f) correspond to $y=0.001395m$, at different horizontal positions in the fluid domain; (g) and (h) correspond to $y=0.00197m$, at different horizontal positions in the solid domain.

Fig. 3 presents the comparison of temperature fields between COMSOL numerical simulations and semi-analytical solutions at different time instances, demonstrating good consistency between the two approaches. Furthermore, the figure reveals the spatiotemporal evolution of conjugate heat transfer induced by the interfacial heat source. During Time II, the interfacial heat source transfers thermal energy to the fluid and solid domains via convective heat transfer and heat conduction, respectively. Due to convective effects, the temperature distributions in both the fluid and solid domains exhibit a left-low, right-high pattern along the flow direction. As the fluid flows through Region II and carries thermal energy to Region III, it heats the solid domain in Region III. Meanwhile, due to the axial heat conduction considered in both energy equations (1) and (3), the solid domain conducts heat axially toward both sides of Region II, heating the fluid in the Region I and Region III. Subsequently, during Time III, the accumulated heat within the solid domain is gradually removed by the fluid through convective heat transfer.

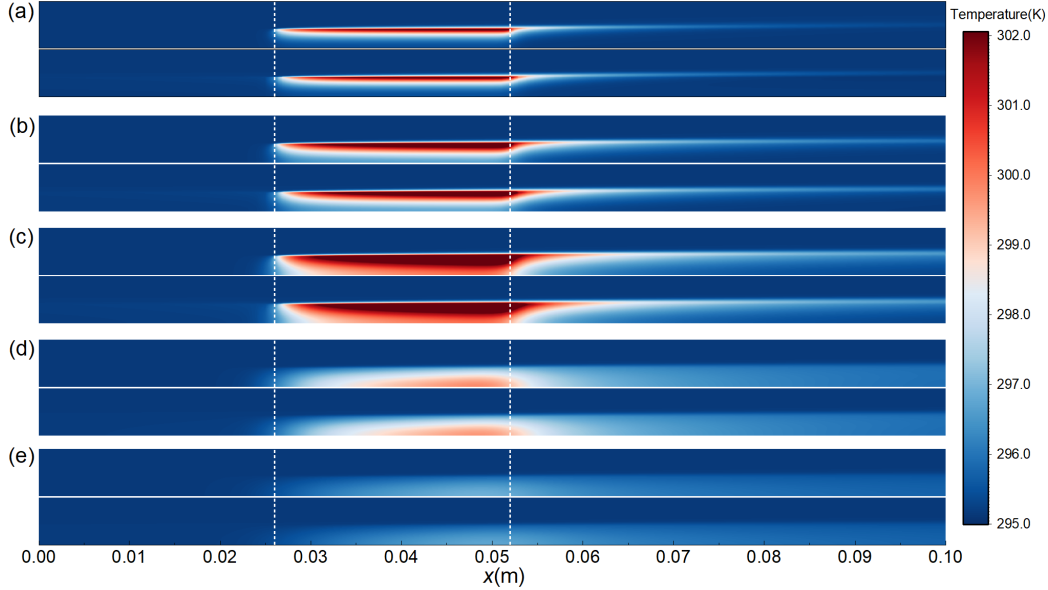


Fig. 3: Comparison of temperature distributions between COMSOL simulations and semi-analytical solutions at various time instances (with the upper figure in each subfigure representing the COMSOL solution and the lower figure representing the semi-analytical solution): (a) $t=1.5\text{s}$; (b) $t=2.0\text{s}$; (c) $t=3.0\text{s}$; (d) $t=5.0\text{s}$; (e) $t=8.0\text{s}$.

3.2. Spatiotemporal flow direction analysis of interfacial heat flow

In the previous section, the spatiotemporal evolution of the transient temperature field shown in Fig. 3 was preliminarily analysed to investigate the heat flux transfer induced by the interfacial heat source. This section will further analyse the spatiotemporal heat flux direction by utilizing the fluid-side interfacial heat flux φ_{wf} obtained through the thermal quadrupole method. The expression for the fluid-side interfacial heat flux $\tilde{\varphi}_{wf}$ in the Laplace domain is as follows:

$$\tilde{\varphi}_{wf} = -\frac{A_s C_f}{C_f A_s + D_f C_s} \bar{I}R \quad (25)$$

By applying the inverse Laplace transform to equation (25), the spatiotemporal heat flux distribution φ_{wf} at the fluid-side interface is obtained and visualized in Fig. 4. The top-left figure shows the fluid-side interfacial heat flux φ_{wf} at different time instances as a function of axial position, while the bottom-right figure shows φ_{wf} at different axial positions as a function of time. When $\varphi_{wf} > 0$, heat flows from the fluid side to the solid side, corresponding to regions above the zero-value iso-heat flux line, highlighted in pink. Conversely, when $\varphi_{wf} < 0$, heat flows from the solid side to the fluid side, corresponding to regions below the zero-value iso-heat flux line, highlighted in green.

Furthermore, for the top-left figure, as time transitions from Time II to Time III (in the figure, t progresses from 2s to 3.3s and then to 5s), on one hand, the heat flux transferred from Region II to the fluid side gradually decreases, while the heat flux transferred from the fluid side to the solid side in Region III also diminishes. On the other hand, the intersection point of the heat flux curve with the zero-value iso-heat flux line gradually shifts to the right, indicating that

the heat flux initially flowing from the fluid to the solid side in Region III eventually reverses direction and flows back to the fluid side until it is carried away by the convective flow. Additionally, due to axial heat conduction in the solid domain, the fluid entering Region II from Region I is preheated.

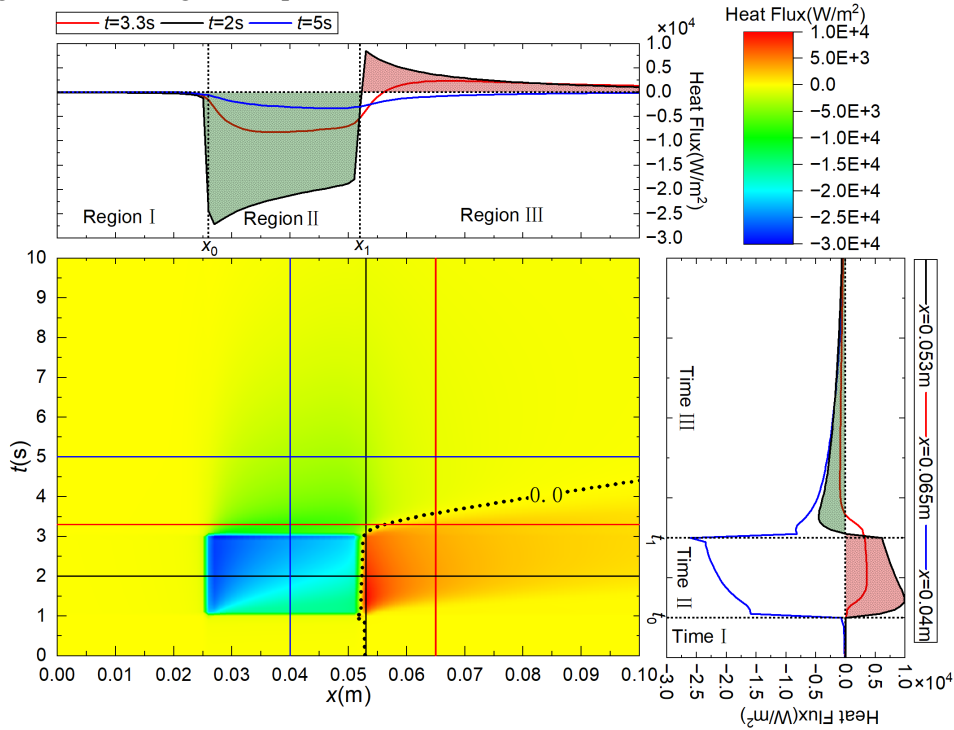


Fig. 4: Spatiotemporal distribution of heat flux at the fluid-solid interface, along with heat flux curves corresponding to different locations and times.

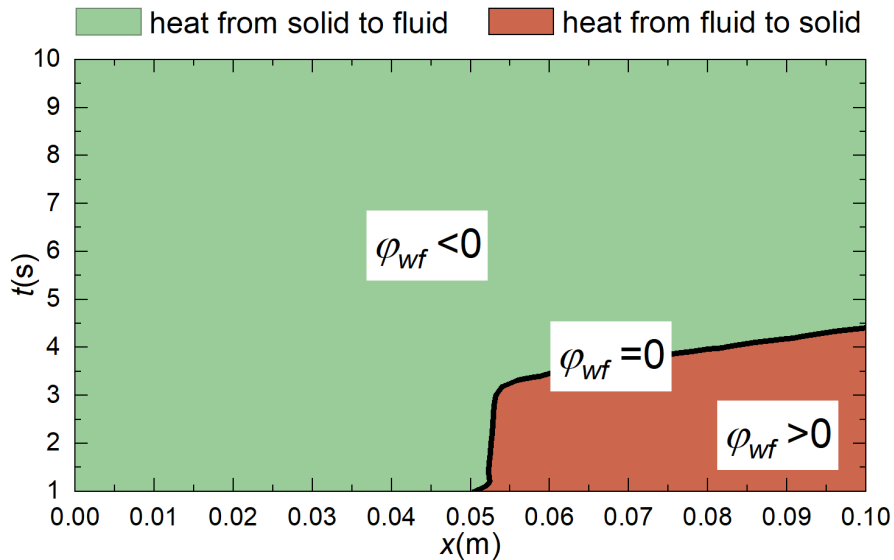


Fig. 5: Spatiotemporal distributions of heat flux direction at the fluid-solid interface

Similarly, from the bottom-right figure, on one hand, during Time II, as the axial position transitions from Region II to Region III (in the figure, x progresses from 0.04m to 0.053m and then to 0.065m), the heat flux direction changes from transferring heat from the solid side to the fluid side to transferring heat from the fluid side to the solid side. On the other hand, during Time III, the intersection point of the heat flux curve with the zero-value iso-heat flux line gradually shifts to the left. While part of the heat flux direction reverses in certain periods, most of the heat flux continues to flow from the solid side to the fluid side, with the magnitude gradually decreasing.

Finally, by extracting the zero-value iso-heat flux line from the spatiotemporal distribution figure of the fluid-side interfacial heat flux, the fluid-side heat flux direction map at the fluid-solid interface was obtained, as shown in Fig. 5. In the figure, the green regions indicate heat flux flowing from the solid to the fluid, while the red regions indicate heat flux flowing from the fluid to the solid. In addition, this figure clearly illustrates the direction of the interfacial heat flux at different times and axial positions.

4. Conclusion

This study investigates the transient conjugate convective heat transfer in a channel induced by an interfacial heat source at the fluid-solid interface. The transient temperature fields in both the solid and fluid domains were obtained using the thermal quadrupole method combined with a two-dimensional numerical Laplace inverse transform technique. The reliability of the semi-analytical solutions was validated through finite element numerical simulations. The primary advantage of the derived semi-analytical solution lies in its ability to efficiently and rapidly calculate the temperature or heat flux density at specific positions and times within the geometric domain, without the need for time-consuming full-domain and full-time calculations. Based on this, the spatiotemporal heat flux directions at the interface were studied using the theoretical solution for the fluid-side interfacial heat flux density, leading to the development of a corresponding spatiotemporal heat flux direction map. This work provides theoretical support and guidance for analyzing transient conjugate convective heat transfer in channels induced by interfacial heat sources.

Acknowledgements

This research was supported by Zhejiang Provincial Natural Science Foundation of China under Grant No. LD24E050008, and the National Natural Science Foundation of China No. 52441504 & 52475076.

References

- [1] T. A. Alves and C. A. C. Altemani, "Conjugate Cooling of a Discrete Heater in Laminar Channel Flow," *J. Braz. Soc. Mech. Sci. Eng.*, vol. 33, no. 3, pp. 278–286, 2011.
- [2] T. A. Alves and C. A. C. Altemani, "Convective cooling of three discrete heat sources in channel flow," *J. Braz. Soc. Mech. Sci. Eng.*, vol. 30, no. 3, pp. 245–252, 2008.
- [3] T. A. Alves and C. A. C. Altemani, "Thermal Design of a Protruding Heater in Laminar Channel Flow," in *2010 14th International Heat Transfer Conference, Volume 2*, Washington, DC, USA: ASME, Jan. 2010, pp. 691–700.
- [4] H. Bhowmik, C. P. Tso, K. W. Tou, and F. L. Tan, "Convection heat transfer from discrete heat sources in a liquid cooled rectangular channel," *Appl. Therm. Eng.*, vol. 25, no. 16, pp. 2532–2542, 2005.
- [5] J. Padet, "Transient convective heat transfer," *J. Braz. Soc. Mech. Sci. Eng.*, vol. 27, no. 1, pp. 74–95, 2005.
- [6] X. Fu, Y. Huang, L. Hu, H. Xie, and W. Chen, "Flow behavior control in immersion lithography," *Flow Meas. Instrum.*, vol. 53, pp. 190–203, 2017.
- [7] Fu X., "Simulation and Experimental Investigation of Immersion Flow Field in Immersion Lithography," *J. Mech. Eng.*, vol. 47, no. 02, p. 189, 2011.
- [8] A. Wei, A. Abdo, G. Nellis, R. Engelstad, J. Chang, E. Lovell, and W. Beckman, "Simulating fluid flow characteristics during the scanning process for immersion lithography," *J. Vac. Sci. Technol. B Microelectron. Nanometer Struct. Process. Meas. Phenom.*, vol. 21, no. 6, pp. 2788–2793, 2003.
- [9] W. P. Winfree, J. N. Zalameda, P. A. Howell, and K. E. Cramer, "Simulation of thermographic responses of delaminations in composites with quadrupole method," presented at the SPIE Commercial + Scientific Sensing and Imaging, J. N. Zalameda and P. Bison, Eds., Baltimore, Maryland, United States, May 2016, p. 98610N.
- [10] S. Chevalier, M. Garcia, A. Sommier, and J.-C. Batsale, "Semianalytical mass transfer impedance model in microfluidic electrochemical chips," Oct. 17, 2022, *arXiv*: arXiv:2210.08867.
- [11] G. Maranzana, I. Perry, and D. Maillet, "MODELING OF CONJUGATE HEAT TRANSFER BETWEEN PARALLEL PLATES SEPARATED BY A HYDRODYNAMICALLY DEVELOPED LAMINAR FLOW BY THE QUADRUPOLE METHOD," *Numer. Heat Transf. Part Appl.*, vol. 46, no. 2, pp. 147–165, 2004.
- [12] P. Den Iseger, "NUMERICAL TRANSFORM INVERSION USING GAUSSIAN QUADRATURE," *Probab. Eng. Information Sci.*, vol. 20, no. 1, pp. 1–44, 2006.